Available online at www.sciencedirect.com
SCIENCE DIRECT®
International Journal of Heat and Mass Transfer 47 (2004) 353–361
International Journal of HEAT and MASS TRANSFER
www.elsevier.com/locate/ijhmt

Experimental shell-side heat transfer and pressure drop in gas flow for spiral-wound LNG heat exchanger

Bengt O. Neeraas [a,*], Arne O. Fredheim [a], Bjørn Aunan [b]

[a] *Statoil Research Center, 7005 Trondheim, Norway*
[b] *PGS Production AS, 7010 Trondheim, Norway*

Received 18 October 2002; received in revised form 25 April 2003

Abstract

A test plant has been constructed for measurements of local heat-transfer coefficients and frictional pressure drops on the shell side of spiral-wound LNG heat exchangers. Measurements have been performed with gas flow, liquid film flow and two-phase shear flow. This paper focuses on the measurements and the results from the gas flow measurements. 221 gas flow heat-transfer measurements and 80 gas flow frictional pressure drop measurements have been performed at a *Re*-number range of 5000–170 000 with nitrogen, methane, ethane and methane/ethane mixture as test fluids.
© 2003 Elsevier Ltd. All rights reserved.

1. Introduction

The most important heat-transfer equipment in base-load LNG plants is the main cryogenic heat exchanger for cooling, condensation and liquefaction of the natural gas. The multi-stream spiral-wound type is the most commonly used heat exchanger for this application. Information regarding heat-transfer and pressure drop models for spiral-wound heat exchangers is proprietary information for the very few manufacturers of such units. To be able to perform design and rating calculations and static and dynamic process simulation of this type of equipment, reliable methods for calculation of heat-transfer coefficient and pressure drop are needed. In a spiral-wound heat exchanger used for LNG production the refrigerant evaporates on the shell side in downward flow. The streams on the tube side are condensing or single-phase natural gas and refrigerant. Two different test plants have been constructed in the laboratories of The Norwegian University of Science and Technology (NTNU) and SINTEF Energy Research in Trondheim, Norway, for the purpose of measuring heat-transfer coefficients and pressure drop, both for shell-side evaporation and tube-side condensation. Based on the measurements, calculation models have been selected or developed.

A principle sketch of a multi stream spiral-wound heat exchanger is depicted in Fig. 1 [1]. The different tubes are coiled in layers around the central core. The coiling direction alternates from one layer to the next. Radial and longitudinal distances between the tubes are held constant by use of space bars. The tubes are connected to tube sheets at both ends of the heat exchanger.

NTNU and SINTEF Energy Research have since 1984 worked with thermal design and laboratory measurements of heat transfer coefficients and pressure drop for LNG heat exchangers. Three Ph.D. theses have been integrated as part of the research program [2–4].

The results from the measurements have been used to choose and develop calculation models for heat transfer and pressure drop. These models are implemented in a design and optimization tool for LNG plants [5], and in a user-added subroutine program for the process simulator PRO/II [6,7].

* Corresponding author. Fax: +47-73-58-43-45.
E-mail addresses: bone@statoil.com (B.O. Neeraas), aof@statoil.com (A.O. Fredheim), bjorn.aunan@trhm.pgs.com (B. Aunan).

0017-9310/$ - see front matter © 2003 Elsevier Ltd. All rights reserved.
doi:10.1016/S0017-9310(03)00400-9

Nomenclature

a	parameter
A	area (m^2)
b	parameter
B_R	estimated uncertainty from systematic error
C_p	specific isobaric heat capacity (J/kg K)
D	diameter (m)
f_A	arrangement factor for inline tube bank
F	friction factor
g	gravity constant (m/s^2)
h	vertical distances between pressure taps (m)
dl	length (m)
dp	derived pressure drop (Pa)
DP_1	measured pressure drop in test section (Pa)
DP_2	measured pressure drop in test section (Pa)
L	flow length of single tube (m)
m	constant
M	mass flux (kg/m^2 s)
n	parameter, number of measurements
N_{lay}	number of tube layers
Nu	Nusselt number
P_l	longitudinal pitch between tube centers (m)
P_r	radial pitch between tube centers (m)
Pr	Prandtl number
Re	Reynolds number
S_R	standard deviation from random errors
S_{in}	in-line radial distance between tube layers (m)
S_{ref}	radial distance between tube layers (m)
Q_{sec}	electrical power supplied to heated test section (W)
$t_{v,p}$	student-t value
T	temperature (K)
u	flow velocity (m/s)
UI	estimated total uncertainty interval

Greek symbols

α	heat-transfer coefficient (W/m^2 K)
ΔT	temperature difference (K)
λ	thermal conductivity (W/m K)
γ	void fraction for average velocity calculation
μ	dynamic viscosity (N s/m^2)
ρ	density (kg/m^3)

Subscripts

a	acceleration
core	central core in heat exchanger
corr	correction
f	fluid, friction
flow	free flow in test section
g	gravity
he	heated area
in	in-line
lam	laminar
R	result
RSS	root sum square
shell	heat exchanger shell
sec	test section
st	staggered
tube	tube
turb	turbulent
v	vapor
w	wall

Abbreviations

C_1	methane
C_2	ethane
N_2	nitrogen
LNG	liquefied natural gas

2. Experimental set-up

2.1. Description of test facility

A flow diagram of the test facility, including main equipment and instrumentation, is shown in Fig. 2. The facility consists of a test circuit, a propane brine circuit and a methane cooling circuit.

2.1.1. Test circuit

The test fluid is circulated through the test heat exchanger [A] as gas, liquid or two-phase flow. When measurements are performed at two-phase conditions, the fluid is separated into a liquid stream and a vapor stream in a drum [B] after the test exchanger. The flow rate is measured for the liquid [G] and vapor stream [D]. The vapor stream is circulated by a gas blower [C] and cooled [E] before it is mixed with the liquid stream at the test exchanger inlet. The liquid phase is circulated with a pump [F]. The gas and liquid flow is controlled by the use of frequency control on the blower and the pump motors. This provides a smooth regulation of the flow rates and vapor fraction through the test heat exchanger. The temperature of the propane brine controls the temperature in the test circuit. The pressure in the test circuit is controlled both by the temperature and by the total inventory.

2.1.2. Propane brine circuit

The liquid and vapor streams in the test circuit are cooled by cold propane [E], [H]. The propane is circulated by a pump [I] and cooled in heat exchange with

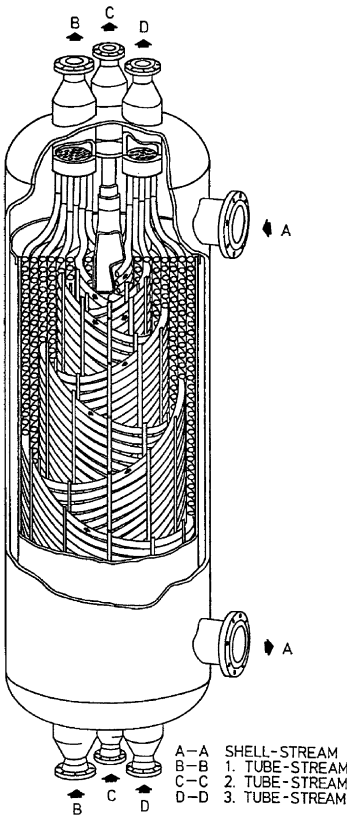

Fig. 1. Principal sketch of a multi-stream spiral-wound heat exchanger [1].

evaporating methane [K]. The brine circuit is branched into three courses; cooling of test fluid liquid phase, cooling of test fluid vapor phase and re-circulation of the brine. The propane flow rate is controlled by frequency regulation of the propane pump motor and the split ratio between the different courses. The brine temperature is controlled by regulation of the capacity of the cryogenerator [N] and by use of an electrical heater [J].

2.1.3. Methane cooling circuit

The main cooling circuit operates by use of thermosyphon circulation. The methane is condensed by the cryogenerator, which provides the refrigeration duty.

The operational ranges for the test facility are given in Table 1.

2.2. Test heat exchanger

A simplified sketch of the test heat exchanger is shown in Fig. 3. The heat exchanger can be operated

Table 1
Operational ranges for test facility

Parameter	Low range	High range
Temperature (°C)	−150	0
Pressure (bar)	1	15
Mass flux (kg/m^2 s)	20	200
Vapor fraction (kg/kg)	0	1
Heat flux (W/m^2)	0	10 000

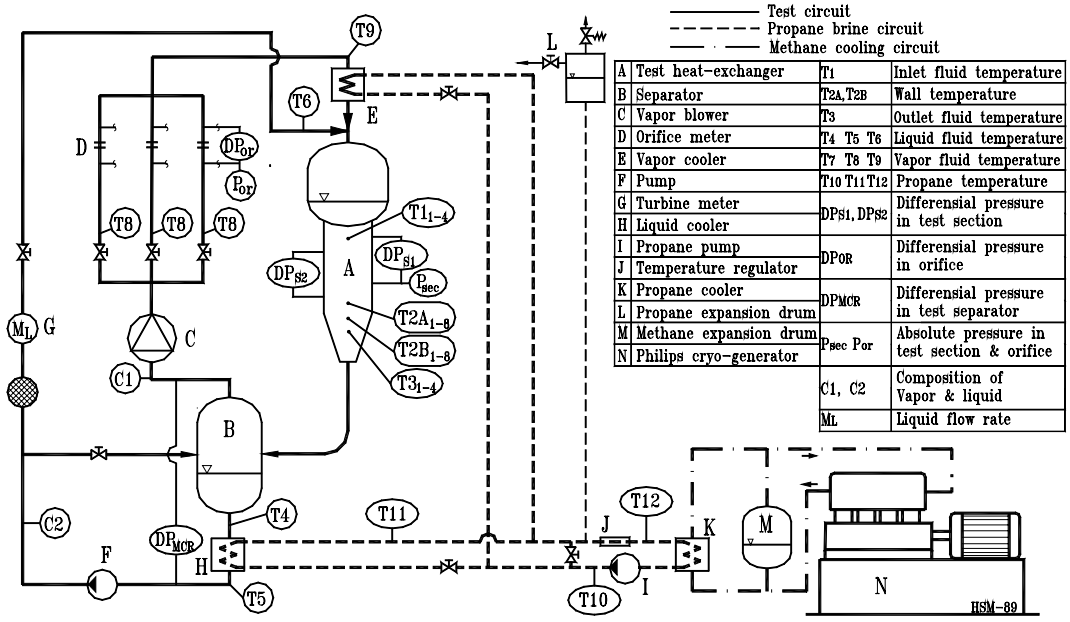

Fig. 2. Flow diagram of the test facility.

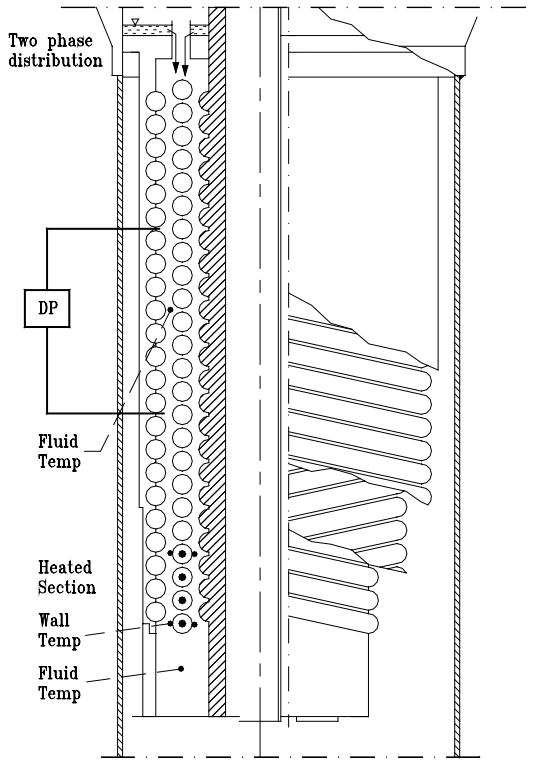

Fig. 3. Test heat exchanger.

both in single-phase and two-phase flow. Before the distribution system the liquid and vapor flow is brought to thermodynamic equilibrium by a mixing system consisting of bends and T-junctions.

It is important to obtain uniform distribution of the two-phase flow in the test exchanger. The flow distribution system consists of a plate with 30 vertical tubes placed in a circle over the central coil. Each tube has two slits, 0.5 mm wide and 100 mm long. The two-phase flow is separated by gravity, and the liquid forms a level over the partition plate before it is drained through the slits in the tubes. The vapor is drained directly through the center of the tubes, and the two-phase flow forms an annular flow pattern through the distribution tubes. The expansion at the outlet of the tubes generates a uniform spray of liquid over the whole flow area in the test section.

The test section is a model of a spiral-wound heat exchanger, and consists of one central coil and two half-tube coils on the inner and outer walls. The center coil contains four parallel tubes and the inner and the outer coils consist of three and five parallel half tubes, respectively. The half tubes on the walls are inserted in order to obtain right flow performance around the center coil where the heat-transfer coefficient is measured. The main layer is coiled to the right and the two half layers are coiled to the left. Three longitudinal space bars are inserted between each of the layers. The tubes in the center coil are also separated by space bars in the longitudinal direction. The test section consists of a flow stabilization zone, an isothermal zone and an electrically heated zone. The tubes in the central coil are electrically heated by heating cables placed inside the tubes. The pressure drop is measured in the isothermal zone and the heat-transfer coefficient is measured in the heated zone. The heated zone is separated from the rest of the heat exchanger by Teflon plugs in order to prevent heat leakage.

2.2.1. Flow area in test section

For calculation of flow velocity in the test section the free flow area has to be calculated. In general the flow area is calculated from Eq. (1) [2].

$$A_{\text{flow}} = \pi \cdot \left[\frac{D_{\text{core}} + D_{\text{shell}}}{2} \right] \cdot N_{\text{lay}} \cdot S_{\text{ref}} \tag{1}$$

S_{ref} is the radial distance between two neighboring tubes and different methods for the calculation exist. The tube configuration varies continuously between in-line and staggered. The in-line configuration gives a minimum radial distance, while the staggered gives the maximum. In the derivation and development of calculation methods for heat-transfer coefficients and frictional pressure drops the in-line flow area, Eq. (2), is applied

$$S_{\text{ref}} = S_{\text{in}} = P_{\text{r}} - D_{\text{tube}} \tag{2}$$

The geometrical data for the test section are given in Table 2.

2.3. Instrumentation and data acquisition

In order to calculate local heat-transfer coefficients and pressure drops, measurements of different para-

Table 2
Geometrical data for the test exchanger

Parameter	Value
Outside tube diameter	12.00 ± 0.05 mm
Longitudinal distance between tube centers	13.94 ± 0.09 mm
Radial distance between tub centers	15.91 ± 0.06 mm
Winding angle	$7.938 \pm 0.06°$
Core diameter (between top of half tubes)	108.0 ± 0.05 mm
Shell diameter (between top of half tubes)	147.63 ± 0.2 mm
Height of test exchanger	336 mm
Vertical distance between pressure taps	126 mm
Height of heated zone	56 mm
Heated tube length	1688.5 ± 3.00 mm
Heated area	63655.0 ± 288 mm^2
In-line flow area	3031.2 ± 63 mm^2

meters have to be done. During operation of the plant some data are taken for control purposes, adjustment and stabilization. The main categories of measurements are; *temperatures*, *absolute pressures*, *differential pressures*, *flow rates*, *heat flux* and *fluid composition*. In Fig. 2 the main instrumentation is shown. An automatic logging system samples data from the different instruments. A Keithley 2001 multi-meter and a Keithley 7001, 80 channel scanner are applied. The raw data are collected in a PC and further processed by a separate data analysis routine.

The uncertainty of measured data as well as thermophysical properties are used to estimate the total measurement uncertainty of derived data such as flow rates, vapor fraction, local frictional pressure drop and local heat-transfer coefficients.

2.4. Treatment of errors

Measured and derived parameters are combined by functional relationships into the result. The estimated errors for each parameter must therefore also be propagated into the results. A result, R, is derived from J number of variables with different average values, x_j; Eq. (3).

$$R = R\langle x_1, x_2, \ldots, x_j, \ldots, x_J\rangle \pm \mathrm{UI} \tag{3}$$

Each x_j may contain both systematic and random errors. The aim is to estimate a total uncertainty interval for the result, and the variables should, as far as possible, be independent of each other.

For the combination of errors, the Root Sum Squares approach is well known and frequently applied, Eq. (4).

$$\mathrm{UI}_{\mathrm{R,RSS}} = \sqrt{B_{\mathrm{R}}^2 + (t_{v,p} \cdot S_{\mathrm{R}})^2} \tag{4}$$

B_{R} is the estimated total error from systematic error sources and S_{R} is the total standard deviation from random errors. For the student-t value, $t_{v,p}$, a 95% probability is used.

A more thorough description of the treatment and propagation of errors are described by Fredheim [2].

2.5. Thermodynamic and physical properties

An in-house software is used for the calculation of thermodynamic and physical properties. The Peng–Robinson equation of state (PR-EOS) [8], [9] is used for thermodynamic calculations.

The density is calculated using a corresponding state method as described by Ely and Hanley [10] and Stephan and Heckenberger [11]. Viscosity and thermal conductivity are calculated by a corresponding state method, similar to the method used for calculation of density. A review of this method can be found from Ely and Hanley [10]. The corresponding state methods were selected because they can handle both pure components and mixtures. The method uses methane as reference fluid.

Table 3
Estimated uncertainty of thermophysical properties

Property	Uncertainty (%)
Specific heat capacity (J/kg K)	±5
Density (kg/m^3)	±2
Thermal conductivity (W/m K)	±8
Viscosity (N s/m^2)	±8

The estimated uncertainty of the used methods is given in Table 3.

3. Data reduction

The heat-transfer coefficient in the test section is calculated from Eq. (5).

$$\alpha = \frac{Q_{\mathrm{sec}}}{A_{\mathrm{he}} \cdot \Delta T} = \frac{Q_{\mathrm{sec}}}{A_{\mathrm{he}} \cdot (T_{\mathrm{w}} - T_{\mathrm{f}})} \tag{5}$$

Q_{sec} is the electrical power supplied to the heated zone of the test exchanger. T_{w} is the average wall temperature in the upper part of the heated zone. T_{f} is the local adiabatic mixing fluid temperature at the same position as the upper wall temperature measurements. T_{f} is calculated from the measured average fluid temperatures at the inlet and outlet of the heated zone, assuming a linear longitudinal temperature profile between inlet and outlet.

The measured pressure drop includes the frictional part, the static part due to gravity and the acceleration part. From the measured values the frictional part is derived, Eq. (6).

$$\mathrm{d}p_{\mathrm{f}} = 0.5 \cdot (\mathrm{DP}_1 + \mathrm{DP}_2) - \mathrm{d}p_{\mathrm{g}} - \mathrm{d}p_{\mathrm{a}} - \mathrm{d}p_{\mathrm{corr}} \tag{6}$$

DP_1 and DP_2 are the measured values from the two pressure transmitters and $\mathrm{d}p_{\mathrm{corr}}$ is to correct for the static head in the impulse line.

The static part of the frictional pressure drop is calculated from Eq. (7).

$$\mathrm{d}p_{\mathrm{g}} = h \cdot g \cdot \rho_{\mathrm{v}} \tag{7}$$

where $h = 0.126$ m is the vertical distance between the pressure taps.

The total pressure drop is measured at isothermal conditions ant the acceleration pressure drop is therefore negligible.

The gas flow rate is calculated directly from the orifice meter based on the measured pressure drop and temperature [12].

Table 4
Operational conditions

Fluid	Temperature (°C)	Pressure (bar)	Flow (kg/m^2 s)	*Re*	*Pr*	n_α	n_{dp}
N_2	−18 to −11	4.6–9.2	6–95	17–69 000	0.70	43	26
C_1	−15 to −9	9.0–14.0	5–85	5–100 000	0.70–0.71	87	45
C_2	−30 to −14	9.3–15.0	5–125	8–170 000	0.77–0.83	76	9
C_1/C_2 45/55 mol%	−16	14.9	7–109	9–139 000	0.75	15	0

4. Experimental results

4.1. Overview of measurements

The experimental results from measurements in gas flow are presented. The range of the measurements by means of test fluid and operational conditions is described in Table 4. A total of more than 200 test runs have been accomplished. To exclude pressure drop measurements with poor measurement accuracy, only measurements with a measured value above 50 Pa are accepted. This is the reason that the number of measurement points presented is fewer for the pressure drop than for the heat-transfer measurements.

4.2. Heat-transfer measurements

All measured Nusselt numbers are shown in Fig. 4. The estimated measurement uncertainty for the local heat-transfer coefficients is given in Fig. 5. The measurement uncertainty is mainly within ±2–8%. The main source for the total uncertainty is the uncertainty of local temperature difference between the test fluid and the tube wall. The measurement points with the highest uncertainty are those with the lowest temperature differences.

For the measurements with methane/ethane mixture as test fluid, selected measured and calculated data is tabled in Table 5.

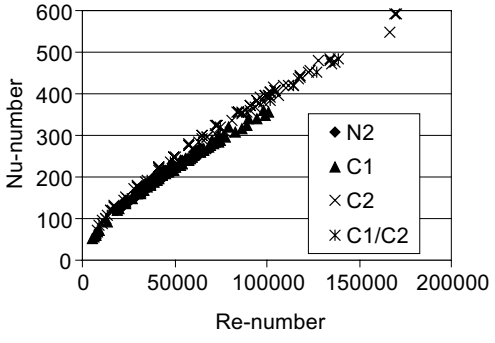

Fig. 4. Measured Nusselt numbers.

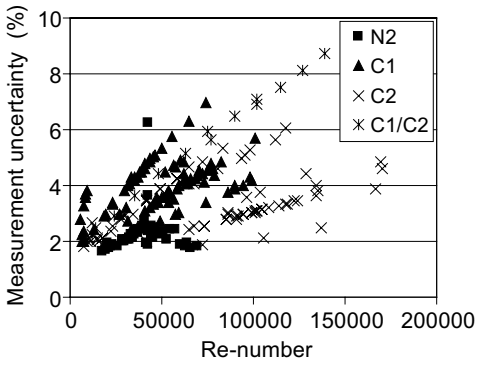

Fig. 5. Estimated measurement uncertainty for heat-transfer coefficients.

4.3. Frictional pressure drop measurements

All measured friction factors are shown in Fig. 6 and the estimated measurement uncertainty for the frictional pressure drops is given in Fig. 7. The measurement uncertainty is mainly within ±1–10%. The measurement uncertainty increases at low *Re*-number due to low measured pressure drop. For some of the measurements with methane as test fluid, selected measured and calculated data is tabled in Table 6.

5. Calculation methods

5.1. Heat-transfer coefficient

For the calculation of heat-transfer coefficient in gas flow a method from Gnielinski [13] for tube banks is applied, Eqs. (8)–(14).

$$Nu = \frac{\alpha \cdot L}{\lambda} = f_A \cdot \left(0.3 + \sqrt{Nu_{lam}^2 + Nu_{turb}^2}\right) \tag{8}$$

$$Nu_{lam} = 0.664 \cdot \sqrt{Re} \cdot Pr^{1/3} \tag{9}$$

$$Nu_{turb} = \frac{0.037 \cdot Re^{0.8} \cdot Pr}{1 + 2.443 \cdot Re^{-0.1} \cdot (Pr^{2/3} - 1)} \tag{10}$$

$$L = \frac{\pi \cdot D_{tube}}{2} \tag{11}$$

Table 5
Data for heat-transfer measurements with methane/ethane mixture

P (bar)	T (°C)	M (kg/m^2 s)	Re	Pr	Nu	α_m (W/m^2 K)
14.956	−15.01	7.40	9402	0.75	83.3	175.1
14.939	−15.11	9.69	12315	0.75	98.6	207.3
14.931	−15.31	10.88	13831	0.75	107.0	224.7
14.912	−15.33	19.04	24197	0.75	149.6	314.5
14.895	−15.56	27.78	35337	0.75	193.2	405.7
14.888	−15.58	37.61	47840	0.75	235.4	494.4
14.880	−15.61	49.67	63172	0.75	283.5	595.3
14.873	−15.55	59.12	75188	0.75	318.1	668.1
14.835	−15.65	60.60	77105	0.75	309.3	649.1
14.844	−15.86	70.24	89428	0.75	357.8	750.3
14.838	−15.71	80.22	102076	0.75	393.5	825.7
14.828	−15.70	80.24	102101	0.75	383.8	805.3
14.821	−15.74	90.17	114766	0.75	419.0	879.0
14.810	−15.89	99.69	126945	0.75	453.7	951.2
14.810	−15.77	108.86	138560	0.75	484.2	1015.7

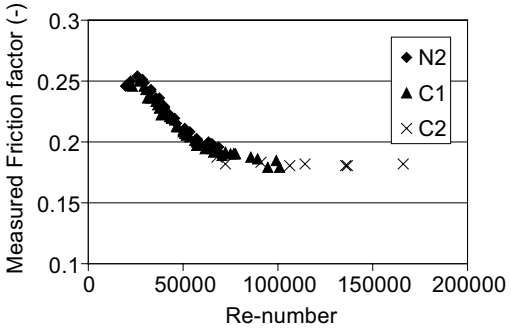

Fig. 6. Measured friction factors.

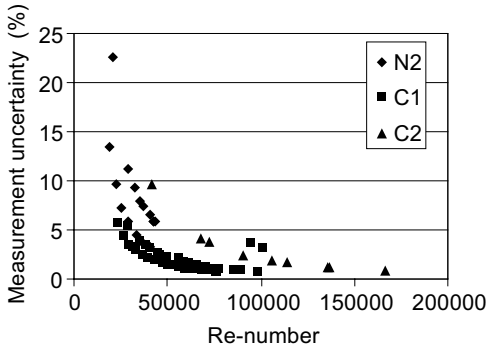

Fig. 7. Estimated measurement uncertainty for frictional pressure drops.

$$Re = \frac{u \cdot L \cdot \rho}{\gamma \cdot \mu} \tag{12}$$

$$\gamma = 1 - \frac{\pi \cdot D_{\text{tube}}}{4 \cdot P_r} \tag{13}$$

$$f_A = 1 + \frac{0.7 + \left(\frac{P_l}{P_r} - 0.3\right)}{\gamma^{1.5} \cdot \left(\frac{P_l}{P_r} + 0.7\right)^2} \tag{14}$$

L is the characteristic length which is the stream length of a single tube, u is the flow velocity in the empty cross section, γ is the void fraction used to calculate the average velocity between the tubes for an in-line tube bank. f_A is the geometry arrangement factor for in-line tube banks.

A comparison between the measured values and the calculated ones by the use of the method from Gnielinski is given in Fig. 8.

As the figure shows, the agreement between the calculated and measured data is very good. A summary of the agreement between the selected calculation model for heat-transfer coefficient and the measured values is given in Table 7.

5.2. Frictional pressure drop

The calculation of the frictional pressure drop is based on a method from Barbe et al. [14], Eqs. (15)–(25), which again is based on a combination of an in-line and a staggered friction factor. It has been chosen to use the in-line flow area for all calculations. Due to this, the constant m used in the calculation of the staggered friction factor has been changed from the original value of $m = 0.27$ to the new value of $m = 0.295$. At Re-numbers above 100 000, the friction factor is found to be constant, and given the same value as at $Re =$ 100 000.

$$\left[\frac{dp}{dl}\right]_f = F \cdot \frac{M^2}{2 \cdot \rho \cdot P_l} \tag{15}$$

Table 6
Data for frictional pressure drop measurements with methane

P (bar)	T (°C)	M (kg/m^2 s)	Re	F	dp_m (Pa/m)
13.664	−11.87	25.00	29390	0.247	526.6
13.660	−11.95	30.23	35542	0.234	729.31
13.667	−11.78	34.35	40377	0.227	915.3
13.671	−11.82	42.69	50184	0.209	1300.5
13.682	−11.67	48.73	57255	0.200	1624.9
13.676	−12.14	52.45	61709	0.194	1824.8
13.686	−12.06	60.22	70831	0.189	2338.7
13.501	−12.20	73.18	86146	0.187	3467.9
13.626	−14.29	80.10	94920	0.179	3898.5
13.659	−13.82	85.32	100929	0.180	4434.6

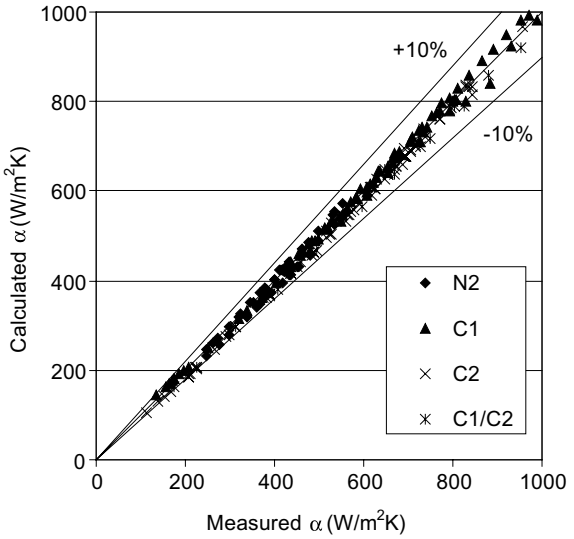

Fig. 8. Measured and calculated heat-transfer coefficients.

Table 7
Deviation between calculated and measured heat-transfer coefficients

Test fluid	Mean deviation (%)	Abs. mean deviation (%)	Standard deviation (%)
N_2	−1.03	2.68	3.26
C_1	0.99	1.81	2.10
C_2	−3.48	3.89	3.12
C_1/C_2	−4.65	4.65	2.13

$$F = \frac{2}{\frac{1}{\sqrt{F_{in}}} + \frac{1}{\sqrt{F_{st}}}} \tag{16}$$

$$F_{in} = \left[\frac{F_{in,0}^2}{F^n}\right] \tag{17}$$

$$F_{st} = \left[\frac{F_{st,0}^2}{F^m}\right] \tag{18}$$

The friction factors F_{in} and F_{st} are calculated by a method from Idel'chik [15]

$$F_{st,0} = 0.88 \cdot \left[\frac{2a-1}{\sqrt{a^2+0.25b^2}} + 1\right]^2 \cdot \left[\frac{2(a-1)}{2a-1}\right]^{1.73} \cdot Re^m \tag{19}$$

$$a = \frac{P_r}{D_{tube}} \tag{20}$$

$$b = \frac{P_l}{D_{tube}} \tag{21}$$

$$Re = \frac{M \cdot D_{tu}}{\mu} \tag{22}$$

$P_r \leqslant P_l$

$$F_{in,0} = 1.52 \cdot (a-1)^{-0.7} \cdot (b-1)^{0.2} \cdot Re^n \tag{23}$$

$n = 0.2$

$P_r > P_l$

$$F_{in,0} = 0.32 \cdot \left[\frac{a-1}{b-1} - 0.9\right]^{-0.68} \cdot (b-1)^{-0.5} \cdot Re^n \tag{24}$$

$$n = 0.2 \cdot \left[\frac{b-1}{a-1}\right]^2 \tag{25}$$

A comparison between the measured values and the calculated ones, by the use of the modified method from Barbe, is given in Fig. 9. As the figure shows, the agreement between the calculated and measured data is very good and better than ±10% for all data points.

A summary of the agreement between the selected calculation model for frictional pressure drop and the measured values is given in Table 8.

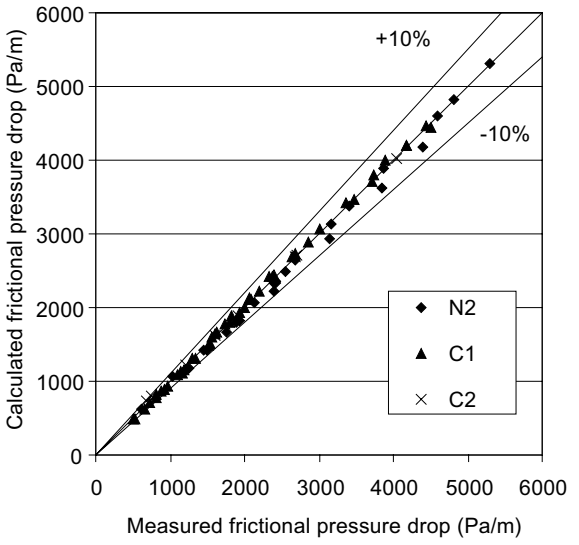

Fig. 9. Measured and calculated frictional pressure drops.

Table 8
Deviation between calculated and measured pressure drops

Test fluid	Mean deviation (%)	Abs. mean deviation (%)	Standard deviation (%)
N_2	−2.67	3.03	2.63
C_1	−0.02	2.03	2.46
C_2	1.68	1.91	2.89

6. Conclusions

Local heat-transfer coefficients and frictional pressure drop for gas flow at the shell side of a spiral-wound LNG heat exchanger have been measured. Based on the measurements, using gaseous nitrogen and various hydrocarbons as test fluids, methods for calculation of heat-transfer coefficients and frictional pressure drop are suggested. Calculated values are compared to the measured ones. The agreement between calculated and measured values is mainly very good.

For calculation of heat-transfer coefficients a method from Gnielinski [13] is recommended. The average deviation is within ±5% compared to the measured values. For the heat-transfer measurements the measurement uncertainty is mainly within ±6%.

For frictional pressure drop a modified method from Barbe et al. [14] is recommended. The average deviation is within ±3% compared with the measured values. For the pressure drop measurements the measurement uncertainty is mainly within ±10%.

Acknowledgements

The work is mainly financed by Statoil Research Center. The technical staff of SINTEF Energy Research and NTNU has done a good effort in the construction, as well as for support during the time of operation, of the test plant.

References

[1] A.G. Linde, Catalogue entitled Rohrbündel-Wärmeaustaucher, Linde A.G. Werksgruppe, TVT, Munich, Germany.
[2] A.O. Fredheim, Thermal Design of Coil-Wound LNG Heat Exchangers, Shell-Side Heat Transfer and Pressure Drop, Ph.D. Thesis, Norwegian Institute of Technology, 1994.
[3] B. Aunan, Shell-Side Heat Transfer and Pressure Drop in Coil-Wound LNG Heat Exchangers, Laboratory Measurements and Modeling, Ph.D. Thesis, The Norwegian University of Science and Technology, 2000.
[4] B.O. Neeraas, Condensation of hydrocarbon mixtures in coil-wound LNG heat exchangers, tube-side heat transfer and pressure drop, Norwegian Institute of Technology, 1993.
[5] G. Owren et al., The LNG plant design optimization tool CryoPro, a joint venture, in: Proceedings of AIChE Spring National Meeting, New Orleans, 1992.
[6] A.O. Fredheim et al., Coil, a model for simulation of spiral wound LNG heat exchangers, in: Proceedings from World Gas Conference 2000, Nice, June 2000.
[7] PRO/II, Steady-state flowsheeting and process optimisation software, Simulation Sciences Inc.
[8] R.O. Peng, D.B. Robinson, A new two-constant equation of state, Ind. Eng. Chem. Fundam. 15 (1) (1976) 59–64.
[9] J.M. Prausnitz et al., Molecular Thermodynamics of Fluid-Phase Equilibria, second ed., PTR Prentice-Hall, 1986, ISMN:0-13-599564-7.
[10] J.F. Ely, H.J.M. Hanley, A computer program for the prediction of viscosity and thermal conductivity in hydrocarbon mixtures, National Bureau of Standards, NBS Technical note 1039, 1981.
[11] K. Stephan, T. Heckenberger, in: Thermal Conductivity and Viscosity Data of Fluid Mixtures, DECHEMA Chemistry Data Series, vol. 10, Part 1, 1987.
[12] DIN 1952, Measurement of fluid flow by means of orifice plates, nozzles and venturi tubes inserted in circular cross-section conduits running full, VDI-rules for measurement of fluid, 1980.
[13] Heat Exchanger Design Handbook, Section 2.5.3 Banks of Plain and Finned Tubes, Bergell House, Inc, 1998.
[14] C. Barbe, D. Mordillat, D. Roger, Pertes de charge en ecoulement monophasic et diphasic dans la calandre des exchangeurs bobines, XII Journees de l'Hydraulique, Paris, 1972.
[15] I.E. Idel'chik, Handbook of Hydraulic Resistance Coefficient of Local Resistance and Friction, 1966.